

# New hysteretic model for wood “frontal” walls

Helena Meireles\*  
Ph.D. student  
Department of Civil Engineering and Architecture (ICIST)  
Technical University of Lisbon (IST)  
Tel.+351 21 841 82 10  
Fax.+351 21 841 82 00  
Email. [hmeireles@civil.ist.utl.pt](mailto:hmeireles@civil.ist.utl.pt)

Rita Bento  
Associate Professor  
Department of Civil Engineering and Architecture (ICIST)  
Technical University of Lisbon (IST)  
Tel.+351 21 841 82 10  
Fax.+351 21 841 82 00

\*corresponding author

## Abstract

The mixed wood-masonry XVIII century *Pombalino* buildings of downtown Lisbon have a recognized patrimonial value both nationally and internationally. These buildings have a three-dimensional timber structure composed of wooden floors, stairs and walls aimed at providing increased seismic resistance and this wooden structure is enclosed in surrounding masonry walls. These interior wooden walls are called “frontal” walls and its behaviour under cyclic loading is very scarcely studied. This report describes, firstly, an experimental campaign to obtain the hysteretic behaviour of these “frontal” walls, by static cyclic shear testing with imposed displacements. A total series of two tests were conducted in two identical real size walls. Secondly, a new hysteretic model for the cyclic behaviour of these “frontal” walls is presented and is calibrated based on the experimental testing results. A hysteresis model was developed based on a minimum number of path following rules that can reproduce the response of the wall under general monotonic or cyclic loading. The model is constructed using a series of exponential and linear functions. There are a total of nine parameters in this model to capture the nonlinear hysteretic response of the wall. The hysteretic behaviour of such walls subjected to cyclic loading exhibit high nonlinear force-displacement responses and high ductility.

## Keywords

Cyclic static shear testing with imposed displacements, hysteresis curve, analytical model

## 1. Introduction

The mixed wood-masonry XVIII century *Pombalino* buildings of downtown Lisbon have a recognized patrimonial value both nationally and internationally. In 1755 a catastrophic earthquake followed by a considerable tsunami stroke the capital of Portugal causing severe damage to the city. The event completely destroyed the heart of the city, which was set on a valley area close to the river Tejo and is composed of a shallow layer of alluvium material. The disaster required an urgent solution. The Prime Minister at the time, Marquis of *Pombal*, was set responsible for the reconstruction of the city and to bring it back to normality as fast as possible. Then, he delegated to a group of engineers the development of a structural solution that would guarantee the required seismic resistance of the buildings. Based on the know-how of that time and on the empirical knowledge gathered from the buildings that survived the earthquake a new construction type was created, this being generally referred to as *Pombalino* construction nowadays. An example of the constructing elements that compose a *Pombalino* building can be seen in figure 1.

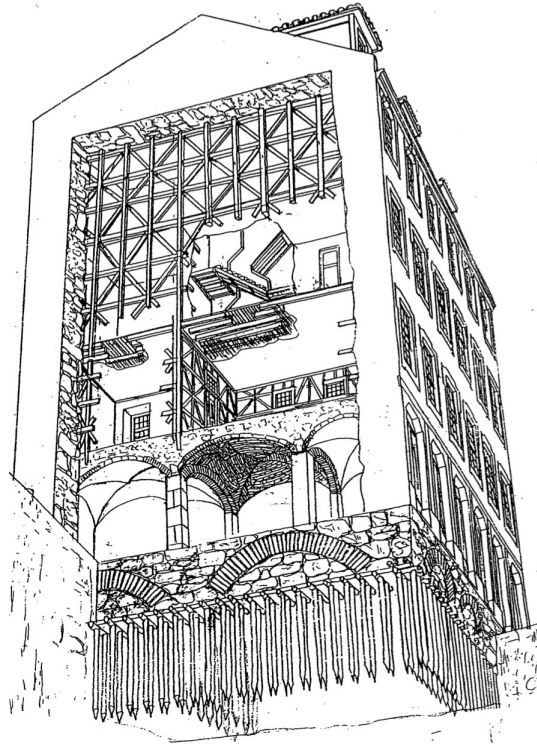


**Fig 1** Example of a *Pombalino* building (Mascarenhas, 2005).

This construction type can be summarized as follows, based on Mascarenhas (2005). The buildings were built in quarters comprising each quarter an average of 10 buildings. The foundation system was ingenious; it is found a system of wooden piles over the alluvium layers. The piles are similar and repetitive, on average 15 cm in diameter and 1.5 m in length. These form two parallel rows in the direction of the main walls, which were linked at the top by horizontal wood cross-members attached by thick iron nails. The construction at ground floor consisted of solid walls and piers linked by a system of arches. In more elaborate cases, thick groined vaults spanned between the arches, which protected the upper floors from the spread of any fire that might start at ground floor level. From the first floor up the basis of the interior of this building system is a three-dimensional timber structure called “gaiola” (cage), thought to be an improved system based on prior traditional wooden houses. The “gaiola” is composed of traditional timber floors and improved mixed timber-masonry shear walls (“frontal” walls) that would support not only the vertical loads but also act as a restraint for the seismic horizontal loading. These “frontal” walls are one of the main speciousness of these buildings. They are made up of a wooden truss system filled with a weak mortar in the empty spaces.

Very few data, analytical and experimental, exists on the behaviour of the “frontal” walls. Such data can be obtained from experiments consisting of physical tests of representative specimen. For this reason it urges to carry out experimental work that can further back up analytical computer models. The experimental activity carried out on these walls so far is limited to Pompeu Santos (1997) and Cruz *et al.* (2001). In the first paper referred, three (although not exactly with the same configuration or dimensions) real site specimen were transported to the laboratory and further tested under reversed cyclic loading with imposed displacements. The study was the first to test such walls under static cyclic shear testing but in these tests no specific loading protocol was used and it is important to mention also that no vertical loading was applied to the structure. These two aspects are seen to be downside of this study. On the second paper mentioned it was intended to assess the possibility and efficiency of using FRP rods and glass fibre fabric, together with epoxy adhesives, in the strengthening of damaged “frontal” walls. What is relevant to point out on this experimental work is that scaled models (1:3) of the wall panels were built and tested in diagonal compression (under monotonic loading). Although these tests are much less time consuming and easy to perform than panel shear tests on real size walls, the data obtained with monotonic testing is preliminary and limited to the most to envelope curves on force-displacement relationships, in this case, of scaled models. For the detailed seismic analysis foreseen for the current study it is required to test the specimen under reversed cyclic loading to obtain the desired hysteresis behaviour of such walls.

The objective of the present research work is divided in to two main parts. The first has been to carry out experimental work to obtain the hysteretic behaviour of the “frontal” walls, by means of static cyclic shear testing with imposed displacements. The test specimen and experimental set-up tries to replicate the construction details, support and boundary conditions and loading conditions that can be found in reality in these buildings. A total of two full scale walls were constructed and tested at the laboratory. Secondly, a new analytical hysteretic model for the cyclic behaviour of these *Pombalino* “frontal” walls is developed and this is calibrated based on the experimental results obtained previously. The analytical hysteretic model has been programmed into a programming software called Matlab (2004).

## 2. Experimental work

### 2.1 Description of the subassembly

A schematic drawing of the wall construction details is shown in figure 3. The intention was to fabricate specimen to test at the laboratory that very much resemble the real size specimens brought to test at the laboratory in Pompeu Santos (1997).

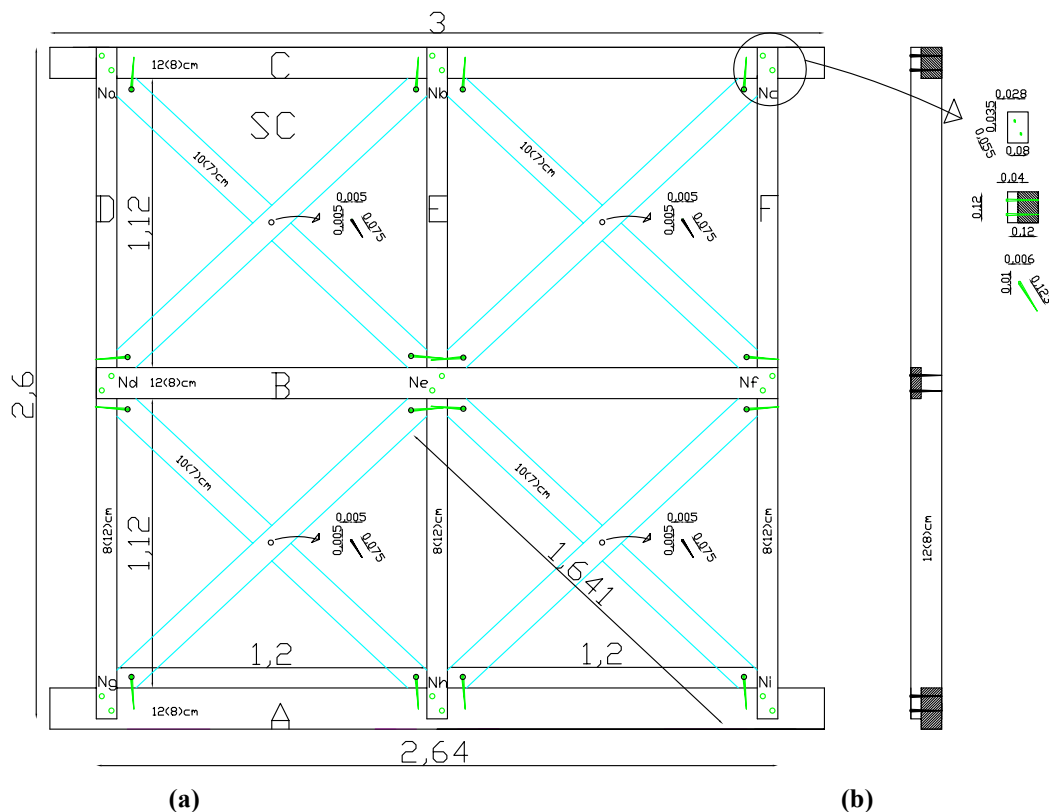


**Fig. 3** Schematic drawing of “frontal” wall specimen and of the details of its connections (units in meters otherwise specified), (a) front view; (b) lateral view.

However, the timber species used may not have been the same and, on the other hand, it is important to notice that, in reality, the section dimensions can vary a lot from building to building. The typical timber species found on the *Pombalino* buildings vary from hardwood species such as Oaks and Chestnuts to softwood species such as Pines. In these old buildings, the softwoods such as Pines seem to be more seldom found. In our case, the timber used in the walls consists of pine ordered from the timber mill. It was ordered a typical softwood Portuguese species (*Pinus Pinaster Ait., Pinho Bravo*). The reasons for selecting this species was that, besides also being found on the *Pombalino* buildings, this is one of the most common species found commercially and therefore easy to find in quantity; hardwood species are harder to find in abundance in the timber mills which inhibits its use. The choice of this *Pinho Bravo* is also due to the fact that this wood specie is the most commonly used timber for structural purposes in new wood buildings in Portugal nowadays.

The woods were ordered dried from green wood to 12% moisture content (the moisture content found in woods at the ambient temperature of 20° and ambient relative moisture of 65%), given that in the old Pombalino buildings the woods have had sufficient time to dry to the ambient moisture content. The wood sections were limited to the common sections found in the timber sawmill: 16x8 cm<sup>2</sup>; 12x8 cm<sup>2</sup> and 10x7cm<sup>2</sup> in section area. Further ahead the wood beams were cut in the carpentry and transported to the university laboratory. In relation to the connections (number of nails, positioning of nails) these were imitated in more detail according to what was possible by the nails existing commercially nowadays. The details of the connections and nails used can be seen in figure 3. The nails used were all pyramidal of 12.5 cm in length by a section of 10x6 mm<sup>2</sup> in the base section. Exceptionally, the nails used to connect the crossed braces among each other are smaller, of 7.5 cm in length by a base section of 5x5 mm<sup>2</sup>. In the main elements a pre-drilling was made of 7.5 mm in diameter only on the upper wood element. To be noted that the nails were bought from a store and were the only ones found, which are still fabricated by handicraft and of forged steel, thus giving a good imitation of what existed in the past. For this reason also the nails can vary slightly in their dimensions (for instance up to 0.5 cm in length and/or up to 0.5 mm in side base section).

Afterwards the walls were mounted as described as follows. First, the elements were set horizontally on the floor and the main elements (all except the crossed braces) were attached together. The nails were nailed manually with a hammer. Later on, the diagonal crossed braces were set in the available space and nailed to the main elements with the longer nails. It was made sure that no empty spaces were found on the connection of the diagonals with the main elements. In relation to the support conditions, to tighten the walls to the horizontal reaction beam, it was built six steel shaped omega flanges (see figure 6) to connect with screws the walls to the horizontal reaction beam, as is further ahead explained. These were set in the proper positions according to the positioning of the holes in the reaction beam. The walls were set vertically to proceed with the filling of the masonry.

The issue of the masonry filling is a problem not easy to solve. It is important to try and reproduce the usual filling that was used for these buildings. However, a great variety of fillings can be found for these walls. From the observations made by companies in rehabilitation or demolition works it has been found different types of masonry such as fillings of typical mortar with bricks or mortar with tiles or even mortar mixed with small stones (which is thought to be the debris or leftovers from the earthquake). For the mortar characterization only one study was found on the type of mortar used (Oz, 1994). This study, based on a collection of real site fragments of mortar from a building under reconstruction, indicates that the used of lime was probably hydraulic; the predominant sand size was between 0.5 to 2 mm and that no particles of cement were found, as it is expected. Furthermore, the relation water/lime was probably superior to 1.0. Based on these observations it was decided that the masonry filling would consist of hydraulic lime with intersections of tiles and broken bricks. A 1.75/2 relation was set for the water/lime relation; a 1/3 relation was set for the lime/sand relation (this is the typical relation used in construction works); as for the sand, a 1/1 relation was set for the sand of river/sand of megrim. Previous studies (Carvalho, 2007) indicate that the mechanical resistance in compression, in accordance with EN1015-11 (1999), of such a composition of mortar does not exceed 1.5 MPa being at 28 days or at 195 days indicating it is a low strength mortar. Three months were the drying time for the masonry.

## 2.2 Description of the experimental set-up

The test specimen described in this section is illustrated in figure 4. Figure 5 presents a photograph of the test frame with a specimen installed and figure 6 shows a schematic drawing of the anchorage system onto the horizontal reaction beam. In figure 6 one can see that the wall SC is anchored to the horizontal reaction beam at the bottom by steel braces in shape of omegas that embrace the lower beam (section 16x8 cm<sup>2</sup>), which are anchored to the horizontal reaction beam by M24 (353 mm<sup>2</sup> in section area) screws, as shown in the figure. The anchorage system is very stiff and can firmly take the shear and moment reactions and avoid the rigid body motion of the wall while loaded (uplift forces). A total of 16 M24 bolts were used.

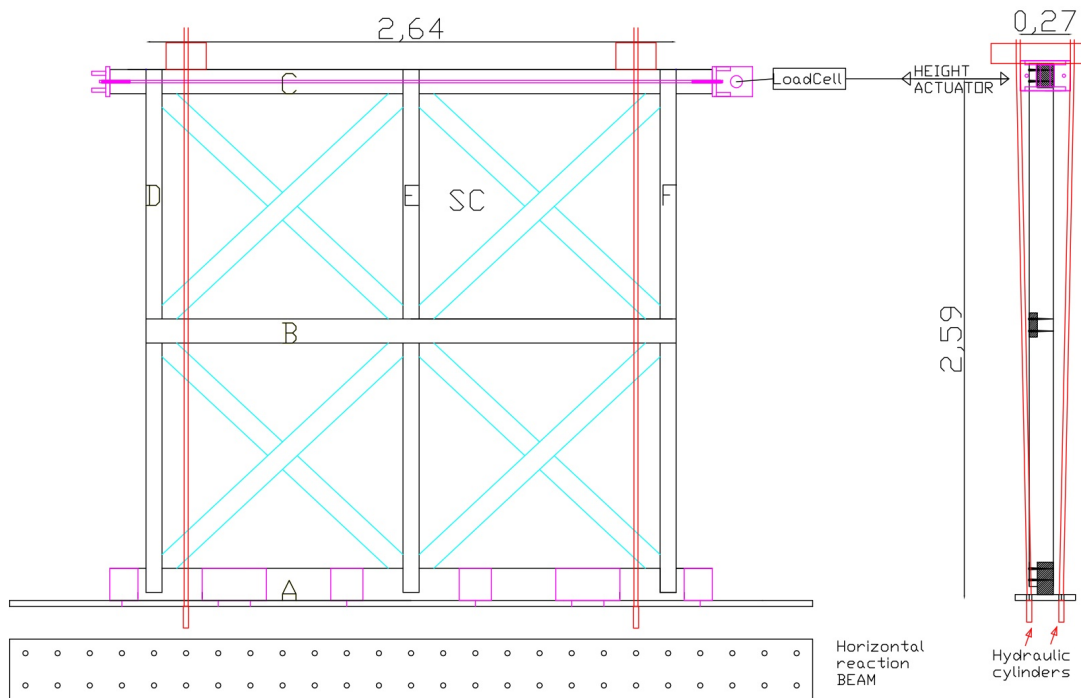


**Fig. 4** Schematic drawing of experimental set-up of specimen SC (units in meters).



**Fig. 5** Photograph of specimen SC mounted with final layout.

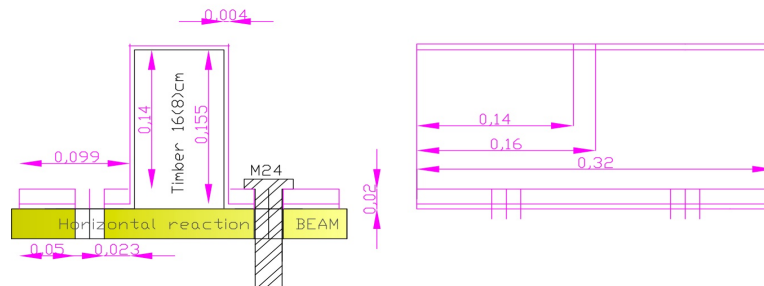


**Fig. 6** Schematic drawing of the anchorage system (units in meters otherwise specified).

The walls were tested with the loading applied at the top of the wall, using a 1000 kN capacity actuator with a 400 mm stroke. Data from two transducers placed on the specimen was recorded. It were recorded the load from the actuator with a load cell and the lateral displacement at the top of the wall via a linear variable differential transducer (LVDT). All data were acquired using a personal computer running Visual Basic. Transverse movement of the specimen during testing (out-of-plane) was resisted by a system of lateral roller bearings (in red in figure 5) supported in a metallic frame (in yellow in figure 5). The weights of the walls are, respectively: 0.756 ton and 0.766 ton.

### 2.3 Loading protocol definition

The CUREE protocol (Krawinkler *et al.*, 2000) for ordinary ground motions was used to study the cyclic behaviour of the “frontal” walls. This protocol consists of cyclic displacement sequences increasing in amplitude throughout the test; each segment consists of a primary cycle with amplitude defined as a multiple of the reference displacement. The primary cycle is followed by a series of cycles with amplitude equal to 75% of the primary cycle. The sequences of the cycle vary in length from 3 to 7 cycles. The input displacements for each of the tests performed can be seen in figure 7. All tests were conducted such that the initial position of the actuator was at half stroke allowing the maximum deflection in each direction (200 mm). The tests were conducted at a rate of 0.25 mm/s. The data were read at a rate of 1mm/sample as well as, in terms of force, at a rate not higher than 0.25 kN/sample.

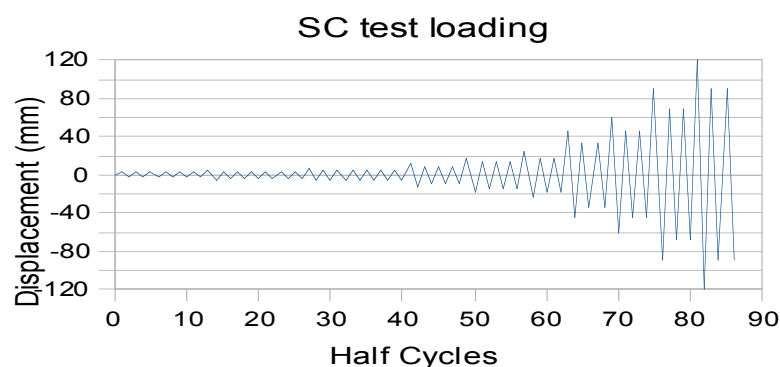


Fig. 7 The loading protocol for the tests performed.

In this case study the calculation of the reference displacement was not done, as it would imply one specimen to be tested under monotonic loading like suggested in the CUREE protocol. Instead, it was set a maximum displacement in the loading protocol equal to the maximum displacement obtained at the LNEC experimental testing (1997), that is 120 mm. Nevertheless, these specimens are one module higher than the ones tested herein; it is for this reason expected that specimens SC2 to SC3 can attain a lower maximum displacement. Accordingly, at experiments of specimen SC2 and SC3 the structures were seen to stand heavy damage at a displacement of around 90 mm. For security reasons in experiments SC2 the experiment was stopped here; nevertheless, in experiment SC3 it was carried out until a displacement of 120 mm since it was the last structures being tested.

### 2.4 Vertical loading

The vertical loading to impose on the test structure was determined based on Eurocode 1 (CEN, 2002) and is given by  $S_d = self\ weight + 0.3 \times live\ load$ . It was considered that the wall was placed at the first floor of a three storey building plus ground floor and attic, so for the calculations of the vertical loads, the dead and live loads defined for a storey were multiplied by three. The area of influence of the walls was considered to be of four meters. For the vertical loads to be imposed on the structure it was considered a live load of 2 kN/m<sup>2</sup> and for dead load it was considered the weight of the compartment walls (0.1 kN/m<sup>2</sup>), the weight of the each wall (3.0 kN/m), the weight of each of the wooden floors (0.7 kN/m<sup>2</sup>) and the weight of each of the ceilings (0.6 kN/m<sup>2</sup>). The output is a total vertical load of 30

kN/m along the wall (per meter of wall). The vertical loading was distributed along 4 hydraulic jacks having each one a total force of 19.2 kN.

## 2.5 Experimental results

The obtained hysteresis curves for specimens SC2 and SC3 are depicted in figures 8, and 9, respectively. The hysteretic behaviour of the “frontal” walls subjected to cyclic loading is characterized by nonlinear behaviour describing the monotonic envelope. It is also observed pinching behaviour associated with strength degradation and generally fat loops can be identified dissipating reasonable amounts of energy. It is also observed a high ductility of the response. The maximum strength of the walls is around 50 kN. The ultimate displacement obtained without collapse of the structure is around 90 mm, resulting in an ultimate drift of around 3.5%.

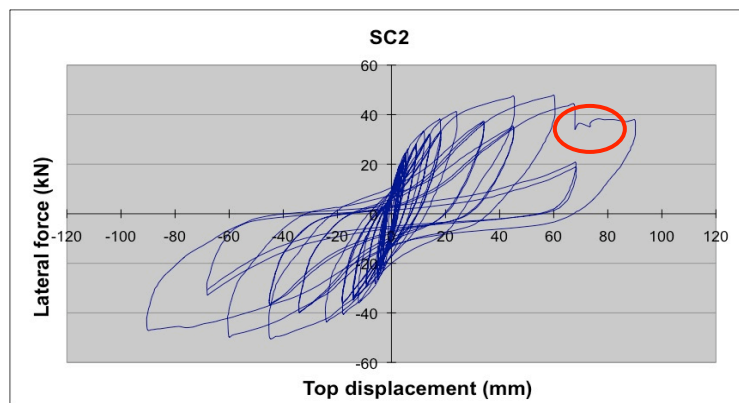


**Fig. 8** Hysteresis curve of wall SC2.

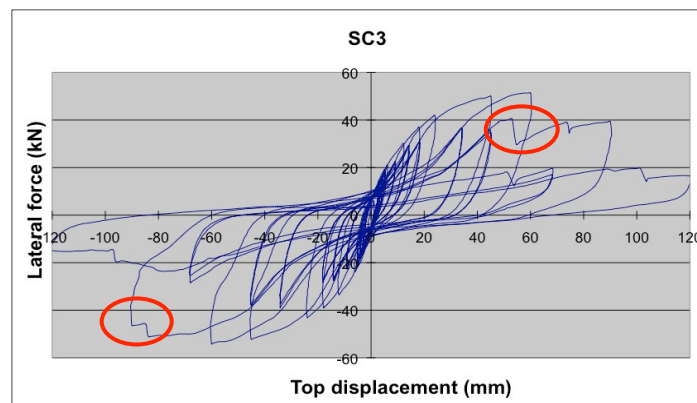


**Fig. 9** Hysteresis curve of wall SC3.

The mode of failure observed in specimens SC2 and SC3 can be seen in figure 10 and is characterized by the buckling and further rupture of diagonals, out-of-plane of the structure. The sudden loss of lateral resistance of the wall when a diagonal ruptures can be observed clearly in the hysteresis curves of figure 8 and 9, marked with red circles.



**Fig. 10** Failure by buckling of diagonal for walls SC2 and SC3.

It is important to refer the resemblance between the results herein obtained for the hysteretic behaviour of the walls built in the laboratory and the results obtained for the hysteretic behaviour of the three site specimen walls tested in LNEC (1997). In terms of general shape of the curves they are the same and in both strength degradation and pinching behaviour is observed. In terms of maximum strength attained, the results are also similar with slight higher strength for the higher real site walls. Finally, in terms of ultimate drift obtained the results are close for the two set of walls tested, being around 3.5%.

### 2.5.1 Effect of the masonry filling

The behaviour of the masonry filling when the structure displays horizontally is further analysed. The following figure is a sketch of a cross diagonal module (the real size specimen tested is composed of 4 modules) at the displacement around collapse. The module is only distorted since when the module is rotated the masonry rotates also but it is not compressed. The original masonry area inside one module has been calculated and is  $1.0356 \text{ m}^2$ . When the panel is distorted the masonry triangles rotate and some of these are compressed. The area of the masonry triangles, which has been compressed, is calculated as  $0.0248 \text{ m}^2$  close to collapse. This value is limited to 2.4% of the total masonry area, which is considered to be a low value indicating low influence of the masonry filling on the strength of the panel. In the following figure it is plotted the undistorted panel in figure 11 (a) and the distorted one (figure 11 (b)) with the area of the compressed masonry filling shown hatched. In red dashed lines are the midsections of the wood elements; at light blue are the diagonals and at pink dashed line is the original size area of the masonry triangles.

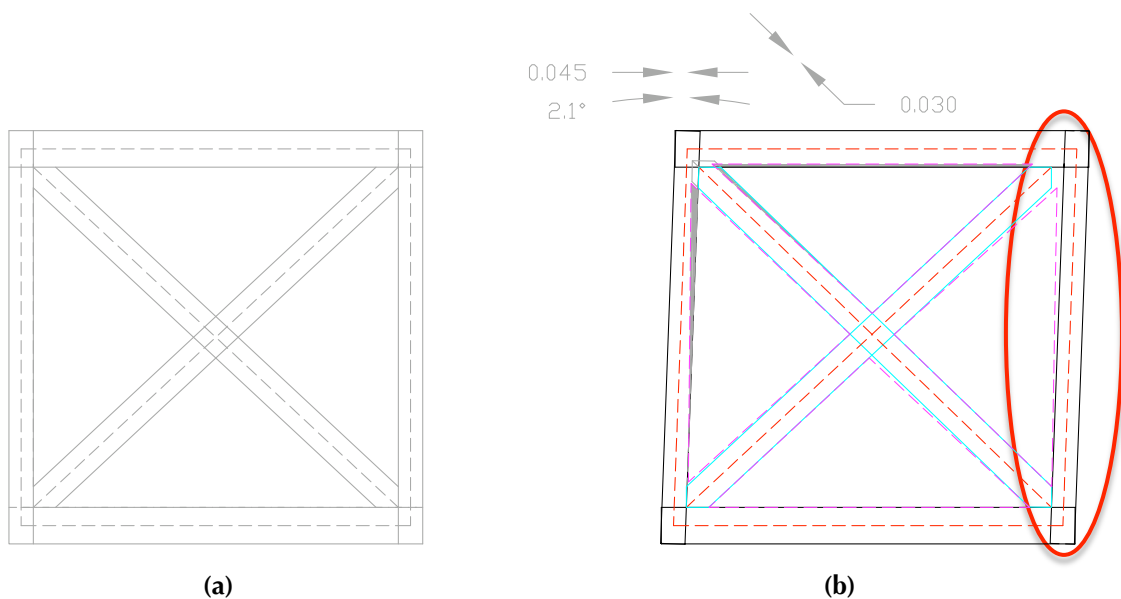


**Fig. 11** (a) Original module (b) distorted module at collapse with compressed area of masonry filling hatched.

On the figure 11 (b) it is also possible to see the detachment of the masonry filling from the timber vertical element on the right and also to see the gap that is formed at the diagonal which is not compressed but loose. Two aspects can be pointed out now. First, it is seen that the diagonal, which is not compressed, is not working under tension but is instead loose. The second aspect is to notice the gap that is formed at the top of this diagonal, which will lead to the pinching effect on the structure. These observations are backed up by the experimental tests and can be seen in picture 12. Herein it can be seen the detachment of the masonry filling from the timber frame, on the right hand side, and the gap opened at the end of the loose diagonal.

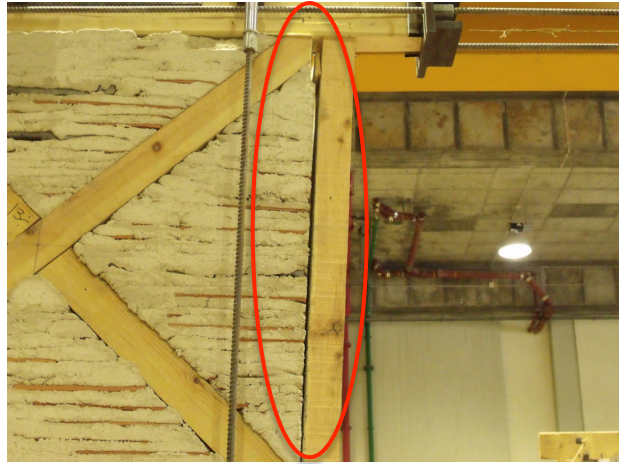


**Fig. 12** Gap between loose diagonal and timber frame and detachment of masonry filling from timber frame.

### 2.5.2 Pinching effect

The obtained hysteresis for the tested walls showed significant pinching effect. Pinching in a structure is usually related to gaps on the structure and residual displacements. We can analyse, as an example, what happens when one loads cyclically two members linked by a connector (any type such as nail, screw, rivet, etc.). Lets assume that the connector is rigid and that the material of the members surrounding the connector is the one being deformed. The following figure 13 sketches how residual displacements and gaps are formed when pulling and pushing the member.

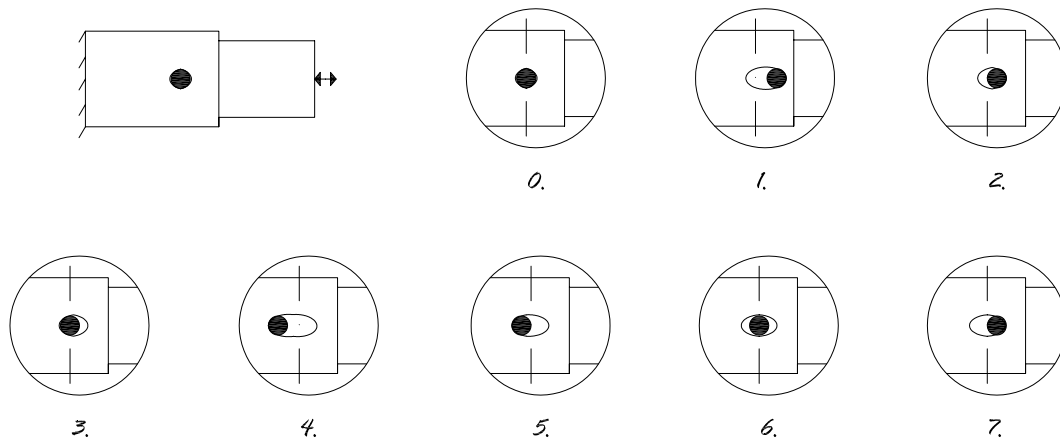


**Fig. 13** Sketch of pinching effect.

If the hysteresis curve for this loading were plotted we would obtain the following hysteretic behaviour (figure 14), where the pinching effect is clearly identified. In figure 14 the numbering used in different paths of the curve corresponds to the one adopted in figure 13.

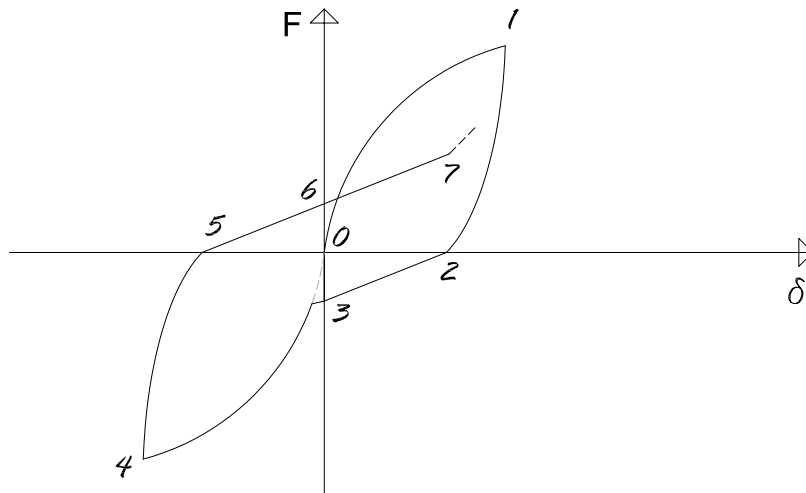


**Fig. 14** Hysteresis behaviour with pinching effect.

The pinching effect is explained as follows:

0. Initial positioning of the connector with no gaps.
1. Pulling of the member. The connector compresses the material to the right and opens a gap at the right.
2. The load starts decreasing until zero. The gap shortens but there are residual displacements and there is a residual gap to the right.
3. Pushing of the member. The connector is taken until the initial position. The load required for this is very low.
4. The connector starts compressing the material to the left side and starts opening a gap on the left.
5. The load starts decreasing until zero. The gap shortens but there are residual displacements and there is a residual gap to the left.
6. Pulling of the member. The connector is taken until the initial position. The load required for this is very low. It can be seen the two residual gaps to the right and left.
7. The connector is taken until the residual displacement on the right. The stiffness required to do this is not the same as the initial stiffness.

A similar effect takes place at the wall panel tested. Gaps are opened between the diagonals and the vertical/horizontal members (see figure 12); gaps are also opened at the connections of the vertical/horizontal members that lead to residual displacements as can be seen on the figure 15. Another important source of pinching might also be associated to the attachment and detachment of the masonry to the timber frame, as can be seen also in figure 12 and figure 11(b).



Figure 15: pull-out of nails leading to the opening of gaps and residual displacements; masonry crack

### 3. Hysteresis model

#### 3.1 Presentation of the model

An hysteresis model was developed based on a minimum number of path following rules that can reproduce the response of the wall tested under general monotonic or cyclic loading. The model was calibrated according to the experimental results obtained. The model is constructed using a series of exponential and linear functions. There are total of 9 parameters in this model to capture the nonlinear hysteretic response of the wall. Figure 16 shows the assumed load-deformation behaviour of the wall.

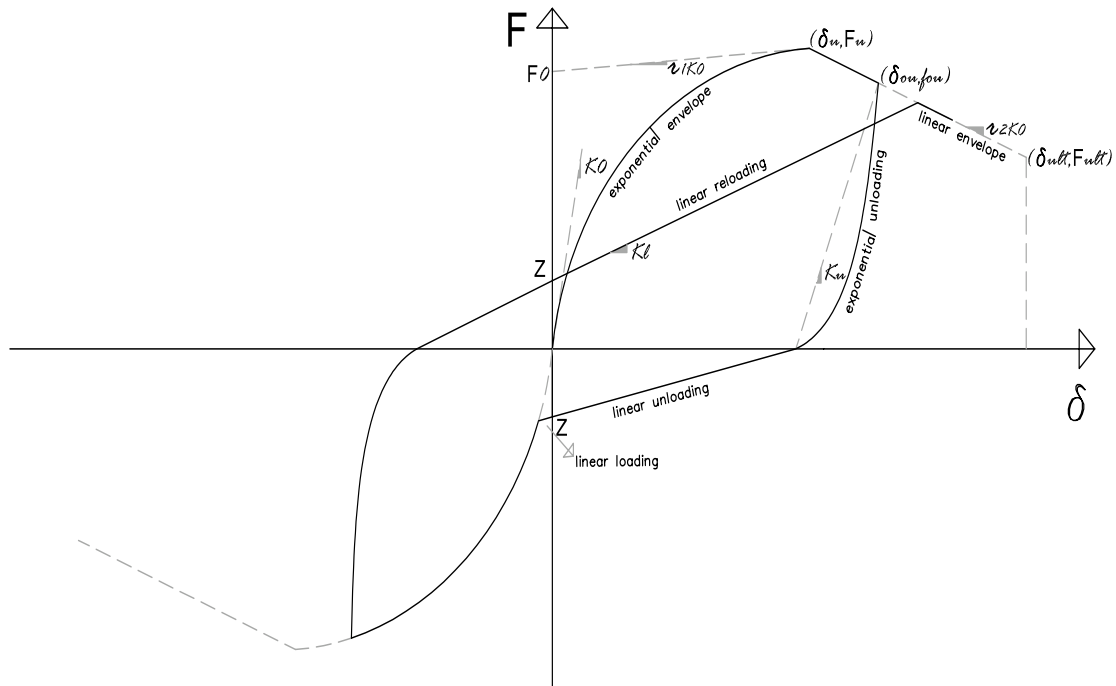


Fig. 16 Hysteresis model.

### 3.2 Path following rules

The first step for obtaining a hysteresis model is to define the envelope curve. It is assumed that the envelope curve is independent of the loading history and coincides approximately with the stress-strain curve obtained under monotonic loading. Once the envelope is determined the loading and unloading paths must be described. Loading (or reloading) paths are identified as cases where both the displacement,  $\delta$ , and the gradient,  $\Delta \delta$ , of the displacement have the same signs ( $\delta * \Delta \delta > 0$ ). In contrast, unloading paths correspond to cases where the displacement and the gradient of the displacement have opposite signs ( $\delta * \Delta \delta < 0$ ).

The paths following rules are such that the structure loaded in the first cycle will draw the envelope curve. It follows an unloading path at a certain point and the loading in the opposite direction. A *linear loading* branch is defined in the model so as to have a transition between the point Z (figure 16) and the envelope curve when the structure is loaded in the opposite direction for the first time. The meaning of Z point will be explained later. Afterwards, when the structure is loaded again in the initial direction, it will reload with a reloading path, which is not the same as the envelope path. When the structure reloading path reaches the envelope curve it means the structure is being loaded for the first time for those displacements; it happens then that the envelope curve is followed again. Again, unloading can happen at any point.

In the following sections, the procedures for constructing the envelope, the loading/reloading and unloading curves within the model are discussed. For clarity of discussion the equations presented in the following sections are exclusively for positive displacement of the hysteretic loops. Implementation of these equations for the negative displacement region implies the reversal of the sign at certain variables and the use of absolute value in others.

### 3.3 Definition of the envelope curves

The monotonic pushover response of the wall is modelled using one exponential and one linear function. The exponential function defines the ascending branch (*exponential envelope*) and the linear function the descending branch (*linear envelope*). The envelope curve is defined by 6 identifiable parameters that must be fitted to experimental data. The parameters, illustrated in figure 16, are  $F_0$ ,  $K_0$ ,  $r_1$ ,  $r_2$ ,  $\delta_u$  and  $\delta_{ult}$ . The respective mathematical functions are the following:

$$F = \begin{cases} (F_0 + r_1 K_0 \delta) \cdot (1 - e^{(-K_0/F_0 \delta)}) & \text{for } \delta \leq \delta_u & (a) \\ F_u + r_2 K_0 (\delta - \delta_u) & \text{for } \delta_u < \delta \leq \delta_{ult} & (b) \\ 0 & \text{for } \delta > \delta_{ult} & (c) \end{cases} \quad (1)$$

The exponential function used to describe the ascending branch (1a) was first proposed by Foschi (1974) and later used by Folz and Filiatrault (2001) in the modelling of wood shear walls response for the CUREE model. Beyond the displacement  $\delta_u$ , which corresponds to the ultimate load  $F_u$  the load-carrying capacity is reduced. Failure of the wall under monotonic loading occurs at displacement  $\delta_{ult}$ . It has been assumed the wall's monotonic deformation capacity  $\delta_{ult}$  is defined as the deformation at which the applied load drops to **80%** of the maximum (ultimate) load  $F_u$  that was applied to the specimen. In this case,  $\delta_{ult}$  is already defined based on  $r_2$ ,  $\delta_u$  and  $F_u$ . So, the number of identifiable parameters is reduced to **5**.

### 3.4 Definition of the unloading curves

Observation of the hysteretic loops of the walls tested in the present work but also on the walls tested at LNEC (1997) reveals a curved shape unloading branch until the zero force intercept and a relatively linear branch from that point until the zero displacement intercept. It also reveals a degrading unloading stiffness if we consider this stiffness to be  $K_u$  in figure 17 ( $K_{u1}$  to  $K_{u3}$ ). This degradation is related to the point of the start of the unloading  $\delta_{ou}$ ; the unloading stiffness  $K_u$  is decreasing with

increasing values of  $\delta_{ou}$ . An exponential function that is capable of capturing this fact has been defined. The mathematical formulation is the following:

$$\begin{cases} F = K_u (\delta - \alpha \delta_{ou}) e^{\lambda_u (\delta - \delta_{ou})} & (a) \\ K_u = \frac{f_{ou}}{\delta_{ou} (1 - \alpha)} & (b) \end{cases} \quad (2)$$

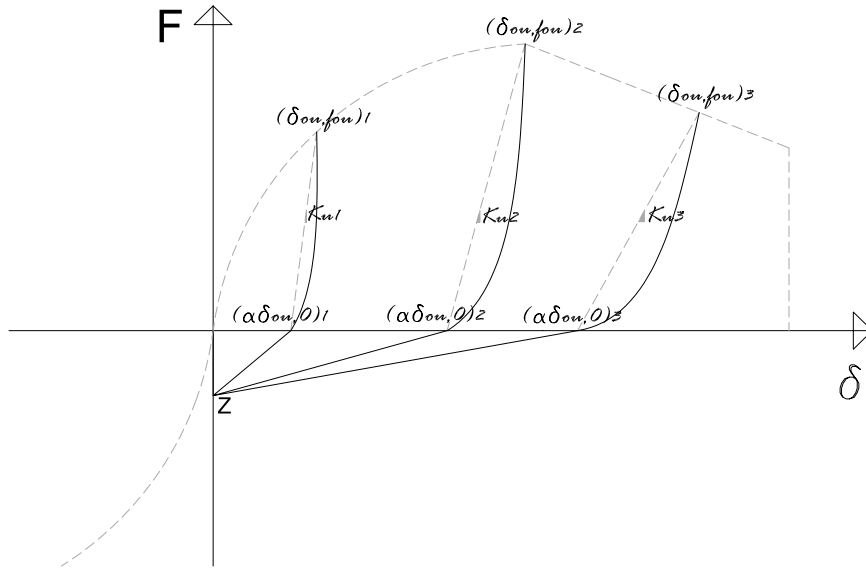


**Fig. 17** Hysteresis model: unloading.

The variables  $\delta_{ou}$  and  $f_{ou}$  are the initial unloading displacement and force, respectively. Equation (2) satisfies the boundary conditions  $F(\delta = \delta_{ou}) = f_{ou}$  and  $F(\delta = \alpha \delta_{ou}) = 0$ . The unloading exponential curve requires the knowledge of 2 identifiable parameters  $\alpha$  and  $\lambda_u$ , which define, respectively, the displacement intercept point and the shape of the exponential curve. These two parameters must be calibrated with experimental data. The parameter  $\alpha$  is fixed for all the loops or for all values of  $\delta_{ou}$ ; on the contrary, the parameter  $\lambda_u$  is not constant and will be a function of  $\delta_{ou}$  as will be explained later. During the unloading process, the variables  $\delta_{ou}$  and  $f_{ou}$  are known and thus are not parameters that need to be defined.

When the unloading starts at point  $(\delta_{ou}, f_{ou})$  it will reach the point  $(\alpha \delta_{ou}, 0)$ . After this a linear function (*linear unloading*) is defined from this point until the point  $(0, Z)$  where the force intercept parameter is called  $Z$ . From the observation of the experimental data we can see that the pinched hysteresis loops do not pass exactly through the same force intercept but are very much close to that. For simplicity of the model it was assumed the same force intercept for all the loops. This parameter,  $Z$ , has to be calibrated with experimental data.

### 3.5 Definition of the reloading curves

One important characteristic that could be observed in the response of these walls is the degradation of the restoring force, commonly known as strength degradation. In this situation, it is observed that the reloading curve does not reach the point of maximum displacement  $(\delta_{max}, F)$  at the envelope curve but instead is pointing to a point that is lower by a certain amount of force (for instance  $a$ ). As a consequence of this the stiffness decreases also by a certain amount or it degrades (stiffness

degradation). In the model defined, the strength degradation was estimated by calculating the force reduction parameter  $\alpha$  for each level of damage. The damage is herein assumed to be related to the maximum displacement (or the maximum drift) attained so far and is a variable that is calculated at each loop based on all the history of the force-displacement response. In this way, a linear reloading curve is drawn from the point  $Z$  to the damaged point that stays below the point  $(\delta_{max}, F)$ . At the beginning of a reloading path the initial point at  $y$ -intercept,  $Z$ , is known. The force reduction parameter  $\alpha$  is calibrated based on the experimental results and is not a fixed parameter, varying with the accumulation of damage on the structure.

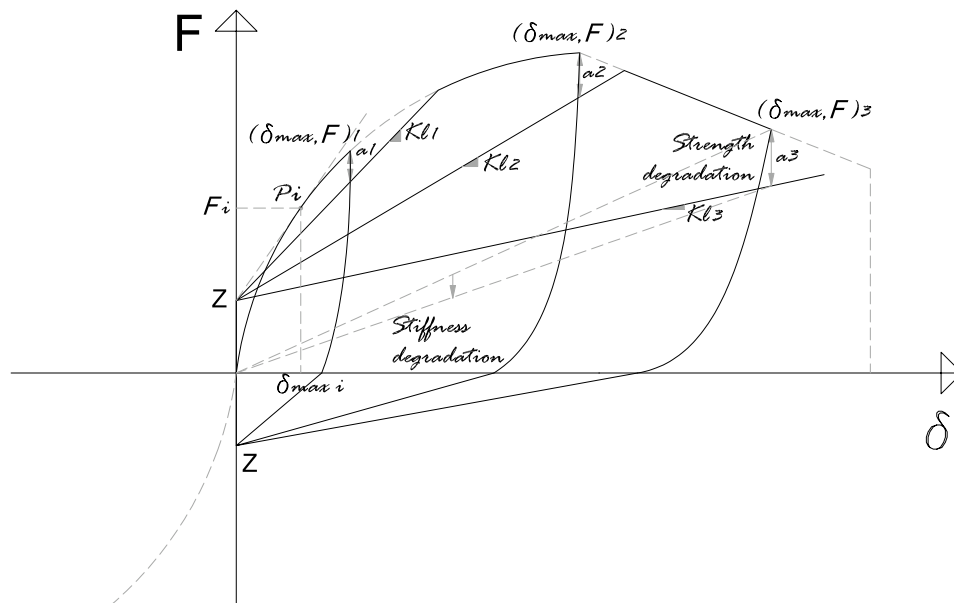


**Fig. 18** Hysteresis model: reloading.

In this way, strength degradation is directly estimated but the stiffness degradation is indirectly accounted for in this modelling technique. In other models, as opposed, the strength degradation is indirectly accounted for.

An aspect related to this modelling is the fact that for all the lower or equal values of damage associated to displacement at point  $P_i$  ( $\delta_{max}^i, F^i$ ) the linear reloading curve will always point to the point  $P_i$  and never to a lower value. It can be said that no damage is seen for this point or before that. Point  $P_i$  is calculated as the point belonging to the envelope curve and the linear function that starts at  $Z$  and is tangent to the envelope curve. This is to avoid that the linear reloading curve has a low derivative for small initial values of displacement, when there is no assumed damage, or even to avoid it from having negative derivatives for very small values of displacement (given that the linear reloading curve starts at  $Z$  and not at origin). As a consequence, the reloading gradient  $K_l$  is constant until the point  $P_i$  and then decreases with increasing damage, see figure 25. The formula for determining  $\delta_{max}^i$  (and thus the point  $P_i$ ) and  $r_l$  at point  $P_i$  is the following:

$$\begin{cases} F^i(\delta_{max}^i) = E^i(\delta_{max}^i) \\ F(\delta_{max}^i) = E(\delta_{max}^i) \end{cases} \Leftrightarrow \begin{cases} r_l K_0 = r_1 K_0 \cdot (1 - e^{-K_0 \delta_{max}^i / F_0}) + (F_0 + r_1 K_0 \delta_{max}^i) \cdot K_0 / F_0 \cdot e^{-K_0 \delta_{max}^i / F_0} \\ r_l K_0 \delta_{max}^i + Z = (F_0 + r_1 K_0 \delta_{max}^i) \cdot (1 - e^{-K_0 \delta_{max}^i / F_0}) \end{cases}$$

$$\Leftrightarrow \begin{cases} r_l = \dots \\ \delta_{max}^i = \dots \end{cases} \quad (3)$$

Where  $F(\delta)$  and  $E(\delta)$  are, respectively, the linear curve that goes from  $Z$  to  $P_i$  and the exponential envelope curve.

### 3.6 Calibration of the parameters

The parameters associated to the hysteresis model must be fitted to experimental data. This can be accomplished by least-square regression of the functions or by the averaging of point parameters.

#### 3.6.1 Force intercept parameter – Z

The force intercept parameter is called  $Z$ . For simplicity of the model it was assumed the same force intercept for all the loops, which is not far away from reality. Based on the experimental data we can plot all the force intercepts, be they positive or negative, and obtain the average point  $Z$ . In figure 19 it can be seen all the force intercepts and the average value obtained for  $Z$  ( $Z=10.16$ ).

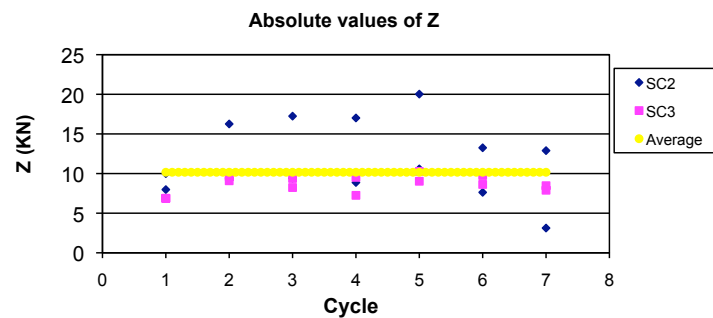


Fig. 19 Average force intercepts point  $Z$ .

#### 3.6.2 Envelope curve parameters - $F_0$ , $K_0$ , $r_1$ , $r_2$ , $F_u$ , $\delta_{ult}$

The values obtained for the envelope curve parameters can be seen in table 1.

Table 1 Envelope curve parameters.

$F_0$ (KN)	37.00
$r_1$	0.04
$K_0$ (KN/mm)	6.1
$r_2$	-0.045
$F_u$ (KN)	50.83
$\delta_{ult}$ (mm)	93.71 (3.78% drift)

As explained before, failure of the wall under monotonic loading occurs at displacement  $\delta_{ult}$ . It has been assumed the wall's monotonic deformation capacity,  $\delta_{ult}$ , is defined as the deformation at which the applied load drops to **80%** of the maximum (ultimate) load  $F_u$  that was applied to the specimen. In this way,  $\delta_{ult}$  is already defined based on  $r_2$ ,  $\delta_u$  and  $F_u$ . This corresponds to an ultimate drift of 3.78%. Accordingly, the couple values of  $(F_u, \delta_u)$  and  $(F_{ult}, \delta_{ult})$  are the following depicted in table 2.

Table 2 Couple values of  $(F_u, \delta_u)$  and  $(F_{ult}, \delta_{ult})$

$\delta_u$ (mm)	56.68	$\delta_{ult}$ (mm)	93.71
$F_u$ (KN)	50.83	$F_{ult}$ (KN)	40.67

The value of  $K_0$  has been taken from the experimental initial stiffness at a displacement of 3 mm. The average value as been assumed based on the SC2 and SC3 test results. The values of  $F_0$  and  $r_1$  have been determined by least-square regression of the function *envelope exponential*. The following figure

20 shows the *exponential envelope* curve for the calibrated parameters and the corresponding experimental points for both negative and positive loading. Herein, it can be seen how well the obtained analytical exponential envelope curve fits the experimental envelope points.

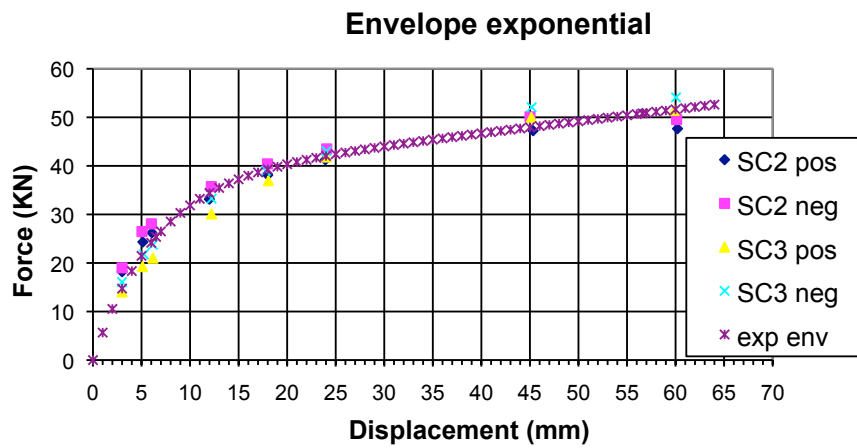


Fig. 20 Exponential envelope curve.

The value of  $r_2$  has been calculated by least-square regression of the function *envelope linear*. Figure 21 shows the *linear envelope* curve for the calibrated parameter,  $r_2$ , and the corresponding experimental points for both negative and positive loading. Herein, it can be seen how well the analytical linear envelope curve fits the experimental envelope points.

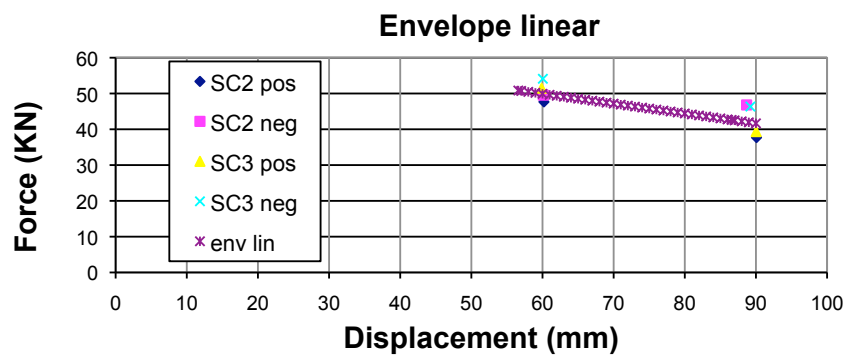


Fig. 21 Linear envelope curve.

### 3.6.3 Unloading curve parameters - $\alpha$ , $\lambda_u$

The value of  $\alpha$  is taken as the average of all the obtained experimental values of  $\alpha$  for positive or negative displacements. The value of  $\alpha$  is estimated as 0.55. The plot of figure 22 shows the values of  $\alpha$  as a function of the experimental unloading points  $\delta_{ou}$  (dou in the plot). Herein, it can be seen how well the value of  $\alpha$  fits the experimentally obtained points.

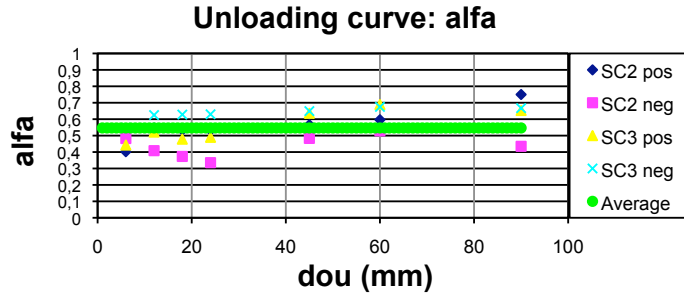


Fig. 22 Estimation of unloading curve parameter  $\alpha$ .

The value of  $\lambda_u$  is the one defining the shape of the unloading exponential curve, as has been seen before. The plot of the values of  $\lambda_u$  as a function of the unloading point  $\delta_{ou}$  (dou in the plot) is shown in the figure 23. Based on these results, it has been decided that the parameter  $\lambda_u$  cannot be a constant value but is better approximated by a logarithmic function dependent of  $\delta_{ou}$  (dou in the plot). The equation for  $\lambda_u$  as a function of  $\delta_{ou}$  (dou in the plot) is given by:

$$\lambda_u = -0.087 \cdot \ln(\delta_{ou}) + 0.4593 \quad (4)$$

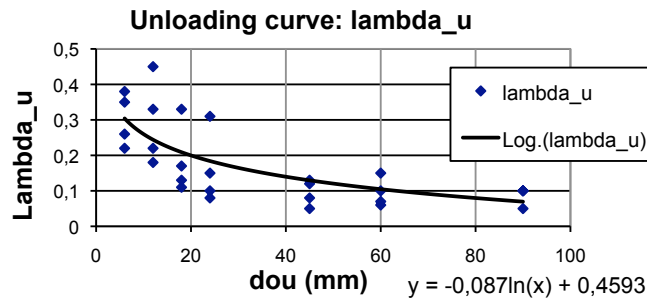
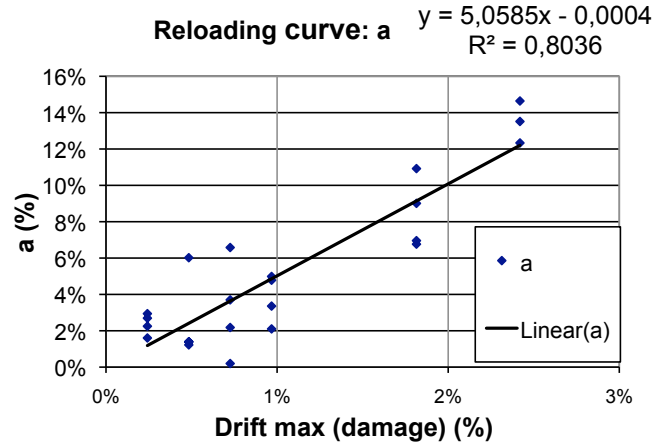


Fig. 23 Unloading curve parameter  $\lambda_u$ .

### 3.6.4 Reloading curve parameter – $a$

In the model defined, the strength degradation was estimated by calculating the force reduction parameter  $a$  for each level of damage. Figure 24 depicts the values of  $a$  obtained experimentally as a function of the maximum drift obtained so far. Herein the damage of the wall is associated to the interstorey drift of the wall. Inter-story drift is a key parameter for the control of damage in wood framed buildings (Filiatrault, 2002). In figure 24, the linear approximation by least-square regression is also presented for the parameter  $a$ . The equation of  $a$  as a function of the damage (maximum drift) of the wall is obtained as:

$$a = 5.0585 \cdot \text{Drift} - 0.0004 \quad (5)$$



**Fig. 24** Parameter  $a$  as a function of the damage.

As a consequence of the previous, we can calculate the reloading stiffness  $Kl$  (or the corresponding coefficient  $rl=Kl/K0$ ). As has been explained previously, the reloading stiffness  $Kl$  (or the corresponding coefficient  $rl$ ) is constant until the point  $P_i$ . In the following plot of figure 25 it is presented the reloading curve coefficient,  $rl$ , as a function of the damage (or the maximum drift). Herein  $rl$  at point  $P_i$  equals 0.375 (and the displacement,  $\delta^i$ , at point  $P_i$  equals 6.5 mm). The values of  $rl$  end for the maximum drift established of 3.8% associated to the collapse of the wall.

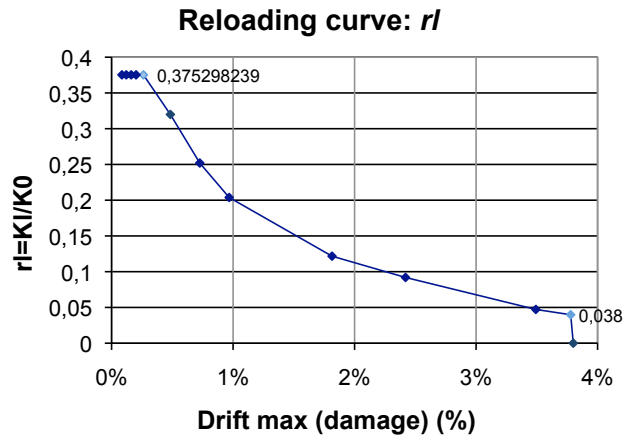


**Fig. 25** Reloading curve coefficient  $rl$  as a function of damage.

## Experimental versus analytical hysteresis

A plot has been drawn for comparison of the hysteresis curves obtained experimentally and the hysteresis curve developed analytically. The hysteresis curve developed analytically has been programmed into the software Matlab (2004). A good matching is obtained as can be seen in figure 26.

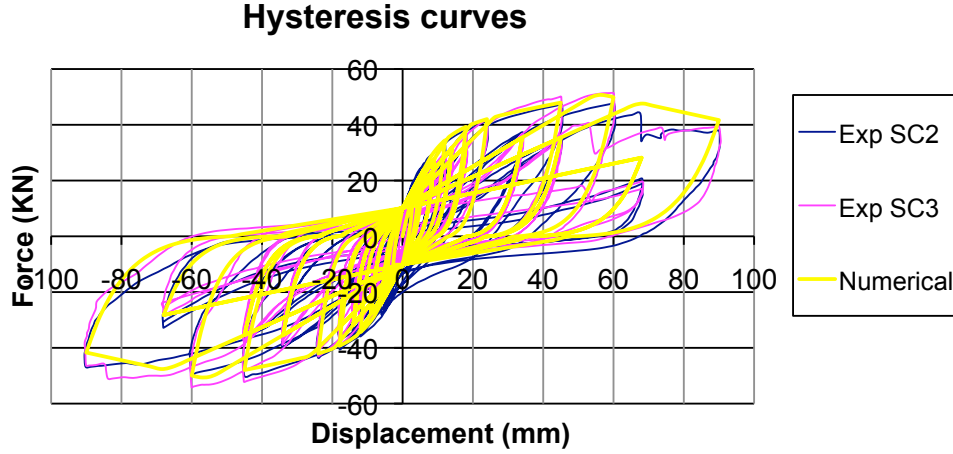


**Fig. 26** Experimental versus analytical hysteresis.

The accuracy of the model response is determined using one error indicator, which is the cumulative energy error (CEE). The CEE is defined as:

$$CEE = \frac{|CE_{test} - CE_{anal}|}{|CE_{test}|} \quad (6)$$

Where  $CE_{test}$  and  $CE_{anal}$  are the cumulative energy dissipation of the hysteresis of the experimental testing and of the analytical model, respectively. The cumulative energy dissipated by the wall,  $CE$ , is calculated as:

$$CE = \sum_i^{\delta_i} \int_{\delta_{i-1}}^{\delta_i} F(\delta) d\delta \approx \sum_i \frac{F_i + F_{i-1}}{2} (\delta_i - \delta_{i-1}) \quad (7)$$

Where the subscript  $i$  is the  $i^{th}$  force-displacement ( $F-\delta$ ) data point. The total percent error in cumulative energy dissipated between the fitted model and the actual cyclic test data is 9% for the test SC2 and 14% for the test SC3, indicating a good match between the analytical and the experimental results.

## Conclusions and further work

The research work presented herein is first focusing on the obtainment of the experimental cyclic behaviour of the so-called “frontal” walls. This has been accomplished through static cyclic shear testing with imposed displacements on such walls. This is top of the art research since very little is known in the literature about the cyclic behaviour of such walls. Nonetheless, the authors believe that further experimental activity is advisable for instance in walls with other dimensions or for other combinations of vertical loading. The obtained results shall output the experimental hysteresis curve via the relation force-displacement. This shall be useful for the development of analytical models for such walls.

The hysteretic behaviour of the “frontal” walls subjected to cyclic loading is characterized by nonlinear behaviour describing the monotonic envelope. It is also observed pinching behaviour associated with strength degradation and generally fat loops can be identified dissipating reasonable amounts of energy. It is also observed a high ductility of the response.

Furthermore, based on the experimental results obtained, a new analytical hysteretic model for wood “frontal” walls has been developed. This is the first hysteretic model developed in the literature for such type of walls. The hysteretic model developed is governed by path following rules and is

composed of linear and exponential functions. It is governed by 9 identifiable parameters. These parameters have been calibrated with experimental test results. The total percent error in cumulative energy dissipated between the fitted model and the actual cyclic test data is 9% for the test SC2 and 14% for the test SC3, accounting the good performance of the model. The model developed also accounts for characteristics such as pinching effect, strength and stiffness degradation that have been observed in these curves.

The results obtained herein are essential for further work in modelling the behaviour of such walls under monotonic or cyclic loading. They are also essential for the further work of the authors in developing a *macro-element* for the structural component: “frontal” walls. This is to be implemented in structural software, called 3Muri ([www.stdata.com](http://www.stdata.com)). This software relates to the analysis of masonry buildings based on a macro-element approach.

## Acknowledgments

The authors would like to acknowledge the financial support of the Portuguese Foundation for Science and Technology (Ministry of Science and Technology of the Republic of Portugal) through the research project PTDC/ECM/100872/2008 and through the PhD scholarship SFRH/BD/41710/2007 granted to Helena Meireles. Also acknowledged is the helpful advice of Prof. Sousa Gago, Eng. Pedro Palma and Prof. Jorge Proença.

## References

- Carvalho J., (2007) Caracterização Mecânica de Paredes Resistentes em Alvenaria de Pedra Através de ensaios não destrutivos; Master thesis, Instituto Superior Técnico (IST) (in Portuguese).
- Eurocode 1: Actions on structures - Part 1-1: General actions -Densities, self-weight, imposed loads for buildings, EN 1991-1-1 (2002) Commission of the European Communities (CEN), Brussels.
- EN 408- (2003) Timber structures- structural timber and glued laminated timber- Determination of some physical and mechanical properties.
- EN12512- (2005) Timber structures- Test methods- cyclic testing of joints made with mechanical fasteners.
- EN1015-11- Methods of test for mortar for masonry (1999) Part 1.1 Determination of flexural and compressive strength of hardened mortar .
- Folz B, Filiatrault A (2001) Cyclic analysis of wood shear walls, Journal of Structural Engineering ASCE, 433-441.
- Filiatrault A, Isoda H, Folz B (2002) Hysteretic damping of wood framed buildings, Engineering Structures 25, 416-471.
- Foschi RO (1974) Load-slip characteristics of nails, Wood Sci., 7(1), 69-76.
- Helena Cruz, José Pedro Moura and José Sporti Machado (2001) The use of FRP in the strengthening of timber reinforced masonry load-bearing walls, Historical Constructions, Guimarães, page 847.
- Krawinkler, H., Parisi F., Ibarra L., Ayoub A. and Medina R (2000) Development of a testing protocol for wood frame structures. CUREE-Caltech Woodframe Project Rep., Stanford University, Stanford, California.
- Mascarenhas J., (2005) Sistemas de Construção; V-O Edifício de rendimento da Baixa Pombalina de Lisboa, Materiais Básicos 3º Parte: O Vidro. Livros Horizonte (in Portuguese).
- Matlab (2004) The Language of Technical Computing, Version 7.0.0.19920 (R14).
- Langlois J.D., Gupta R., Miller T.H. (2004) Effects of Reference Displacement and Damage Accumulation in Wood Shear Walls, Journal of Structural Engineering ASCE,
- OZ Empresa Lda, (1994) work developed for Intergaup, Levantamento e Apoio à Modelação estrutural dos Edifícios do BCP da Rua Augusta e Rua dos Correeiros em Lisboa (Caracterização dos materiais) (in Portuguese) .
- Pompeu Santos, (Julho 1997) Ensaios de Paredes Pombalinas. Nota Técnica N°15/97, NCE/DE, LNEC Lisboa (in Portuguese).
- Pompeu Santos, (1999) Laboratory Tests on Masonry walls taken from an Ancient Building in Lisbon. Procc. of the 34<sup>th</sup> Meeting of CIB W023 Commission in October 1997 in Lisbon, CIB Publication 231, pg. 89-94.
- 3Muri Program release 3.2.11 <http://www.stadata.com> (solver algorithm developed by Lagomarsino S., Galasco A., Penna A.)